Enhancing performance of polar InGaN-based thin film solar cells through intrinsic layer impact optimization

Numerical modeling

El Ghazi, Haddou; Eker, Yasin Ramazan; En-nadir, Redouane; Zaki, Shrouk E.; Basyooni, Mohamed A.

DOI
10.1016/j.rineng.2024.101909

Publication date
2024

Document Version
Final published version

Published in
Results in Engineering

Citation (APA)
El Ghazi, H., Eker, Y. R., En-nadir, R., Zaki, S. E., & Basyooni, M. A. (2024). Enhancing performance of polar InGaN-based thin film solar cells through intrinsic layer impact optimization: Numerical modeling. *Results in Engineering*, *21*, Article 101909. https://doi.org/10.1016/j.rineng.2024.101909

Results in Engineering 21 (2024) 101909

Contents lists available at ScienceDirect

Results in Engineering

journal homepage: www.sciencedirect.com/journal/results-in-engineering

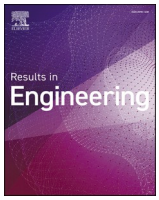

Enhancing performance of polar InGaN-based thin film solar cells through intrinsic layer impact optimization: Numerical modeling

Haddou El Ghazi [a,**], Yasin Ramazan Eker [b,c], Redouane En-nadir [d], Shrouk E. Zaki [e], Mohamed A. Basyooni-M. Kabatas [f,g,h,*]

[a] MPIS Group, ENSAM Laboratory, Hassan 2 University, Casablanca, 20670, Morocco
[b] Science and Technology Research and Application Center (BITAM), Necmettin Erbakan University, 42090, Konya, Turkey
[c] Department of Basic Sciences, Faculty of Engineering, Necmettin Erbakan University, 42090, Konya, Turkey
[d] LPS, Faculty of Sciences, Sidi Mohamed Ben Abdellah University, Fes, 30000, Morocco
[e] Department of Imaging Physics (ImPhys), Faculty of Applied Sciences, Delft University of Technology, 2628, CJ Delft, the Netherlands
[f] Dynamics of Micro and Nano Systems Group, Department of Precision and Microsystems Engineering, Delft University of Technology, Mekelweg 2, 2628, CD Delft, the Netherlands
[g] Department of Nanotechnology and Advanced Materials, Graduate School of Applied and Natural Science, Selçuk University, 42030, Konya, Turkey
[h] Solar Research Laboratory, Solar and Space Research Department, National Research Institute of Astronomy and Geophysics, Cairo, 11421, Egypt

ARTICLE INFO

Keywords:
Photovoltaic
(In, Ga)N
PIN
Solar cell
Performance
Intrinsic layer

ABSTRACT

The paper deals with the conception and feasibility of the device structure based on the optimized PIN-(In, Ga)N homojunction solar cells. A new and efficient model combining the most realistic ones considering the impacts of band gap narrowing, collection efficiency, Shockley-Read-Hall recombination, and interface polarization is proposed to examine the solar cells' performance numerically. The functioning processes of n-$In_{0.42}Ga_{0.58}N$/i-(In, Ga)N/p-$In_{0.42}Ga_{0.58}N$ solar cells at room temperature were investigated by calculating their characteristics for the AM1.5D, AM1.5G, and AM0 American Society for Testing and Materials experimental data. Our results show that the indium content, thickness, and defect density of the intrinsic layer strongly influence the characteristics of the InGaN solar cells. As the In-mole fraction increases, V_{oc}, *FF* and efficiency diminish to reach an independent regime for high In-content. A higher-quality $2\mu m - In_{0.43}Ga_{0.57}N$ for $10^{14} cm^{-3}$ defect concentration can exhibit as high an efficiency as ≅ 11.3%, dropping to ≅ 4.12% for $10^{16} cm^{-3}$ one.

1. Introduction

Renewable energy is a critical topic that must be addressed to solve many issues, such as environmental and energy use. This type of energy has the potential to work out numerous matters related to the current production scheme, which is primarily based on fossil fuels. Solar energy is regarded as the best alternative for dealing with the problems caused by fossil fuels owing to its availability and ease of implementation [1–3]. Today, the leading and most rapidly expanding manufacturing industry is extracting limited energy resources. Abundant solar energy can meet the world's vast energy demands. According to the European Photovoltaic Industry Association (EPIA), solar energy production will reach 1845 GW by 2030, powering 4.5 billion people, mainly in industrialized nations [1]. By the end of 2021, overall global set-up photovoltaic (PV) installations had surpassed 940 GW, up from 772 at its beginning. It increased from 230 GW in 2015 to only 40 GW in 2010 to reach such a level. During the last decades, the increasing rate is about 2250% [2]. In a short period, worldwide energy consumption would grow to 10 TW (TW) per year, and it is expected to reach 30 TW in just over twenty-five years [2]. To lower the CO_2 levels in the earth's atmosphere by 2050, the world would require approximately 20TW (Tera Watt) of non-–CO_2–related energy [3]. Because of the numerous materials and structures available, reducing the fabrication cost, time, and complexity of solar cells has become required. These manufacturing challenges can be overcome by acquiring insight into the devices' functioning and behavior through appropriate simulation software applications and

* Corresponding author.
** Corresponding author.
E-mail addresses: hadghazi@gmail.com, Elghazi.HADDOU@ensam-ca.ma (H. El Ghazi), m.a.basyooni@gmail.com, m.kabatas@tudelft.nl (M.A. Basyooni-M. Kabatas).

https://doi.org/10.1016/j.rineng.2024.101909
Received 16 January 2024; Received in revised form 3 February 2024; Accepted 8 February 2024
Available online 10 February 2024

modeling. The III-nitride semiconductor materials, involving their alloys, are direct bandgap materials encompassing the whole visible range of the solar spectrum. Mainly, InGaN ternary is a good traveler on the road to forthcoming high-efficiency solar cells because it permits coverage of the entire solar spectrum via adjustments in its Indium composition [4,5]. Moreover, InGaN has a high absorption coefficient of $10^5 cm^{-1}$ [6–8], a substantial radiation resistance [9], allowing it to operate in harsh environments, increased carrier mobility, excellent thermal conductivity, as well as low effective mass, which renders it a promising material for solar photovoltaic [7–19]. For instance, Wahab et al. [20] reported an $In_{0.59}Ga_{0.41}N$-related PIN optimum cell efficiency of 19% corresponding to SC characteristics equal to $V_{oc} = 0.875V$, $J_{sc} = 27.36mA.cm^{-2}$ and $FF = 79.39\%$. Also, Feng et al. [21] have conducted a numerical investigation of PIN SC performance, reporting that the high-quality $In_{0.75}Ga_{0.25}N$ SC with a $4\mu m$ i-layer thickness can achieve a high conversion efficiency of 23%. Experimentally, Fellip et al. [22] reported the effects of In-content on the SC electrical characteristics of PIN InGaN homojunctions synthesized by plasma-assisted molecular beam epitaxy. They demonstrate a peak of external quantum efficiency (EQE) of $14 \pm 2\%$ in the blue-to-orange spectral region and extended cut-off up to 600 *nm*. Moreover, (In, Ga) N-based homojunctions obtained by metalorganic vapor phase epitaxy (MOVPE) achieve promising performance (peak external quantum efficiency $EQE = 33\%$) but with a spectral cut-off limited around 420 *nm* [23,24]. Despite significant efforts to research nitride-based photovoltaics [25,26], InGaN solar cells are showing conversion effectiveness of less than 4% for both InGaN/GaN DHJ [26] and p-i-n homojunction devices [27] owing to critical material concerns such as p-type doping, crystal quality, and polarization effects.

The main objective of this paper is to investigate the impacts of different external and internal parameters of the intrinsic layer on the p-i-n SC photovoltaic performance. For this purpose, other SC characteristics such as absorption, collection efficiency, short current density, open circuit voltage, fill factor, and conversion efficiency are reported concerning Content, defect concentration, and thickness of the unintentionally doped layer. The remainder of this paper is organized as follows: Section 2 outlines the physical modeling methodology for the PIN-based InGaN solar cell buildings and addresses their main model elements and required material parameters. The numerical results are presented and discussed in section 3, and some essential conclusions complete the paper.

2. Theoretical background

Compared to a PN diode, the PIN solar cells present some benefits. Given that reverse current breakdown restricts PN diode achievement, a thin intrinsic layer (i-layer) or absorption layer can boost the built-in electric field and entirely deplete the charge carriers, resulting in a substantial prompt current and high quantum efficiency [21]. Excess electrons are donated from the n-type layer to the p-type layer in this structure, leaving the layers positively and negatively charged (respectively) and generating a significant "built-in" electric field (typically an order of magnitude of $10^5 V.cm^{-1}$). As an intrinsic layer is inserted between the (skinny) n and p regions, the depletion region size is the most significant fraction of the total solar cell thickness. Carrier collection in the depletion region is now aided by the electric field, which contributes to making up for the low lifetimes of some materials, such as amorphous silicon. Consequently, the i-layer thickness, defect, and chemical composition are the critical parameters that influence extensively the efficiency of PIN-related solar cells. The solar cell characteristics were derived from the In-mole fraction, size, and defect density using Python code for the incident light intensity of solar radiation related to AM1.5G, AM1.5D, and AM0. The mathematical modeling employed during this paper to execute the device models and improvements presented in the following sections was designed with as few approximations as possible and was based on real-world measurements as often as feasible using in-house written Python code. The following section summarizes it.

The generation of electron-hole pairs via absorbing sunlight is critical to the proper functioning of solar cells. Fundamental absorption is the direct excitement of an electron from the valence band to the conduction band (leaving a hole behind) [28]. Modeling InGaN-based SC necessitates the development of a highly accurate model of light absorption across the entire solar spectrum and for all x-Indium contents. For that reason, we used the following phenomenological model for InGaN that had been suggested previously [28]:

$$\alpha(E,x) = 2.2\ 10^5 \sqrt{a(x)\left[E - E_g(x)\right] + b(x)\left[E - E_g(x)\right]^2} \quad \left(cm^{-1}\right) \tag{1}$$

Where: E is the photon energy, $a(x)$ and $b(x)$ are the Indium-mole fraction-related coefficients. For this absorption modeling, $a(x)$ and $b(x)$ are taken from the experimental reported results in Ref. [29]. We have approximated their In-mole dependency by a polynomial adjustment of the fourth degree for the first and quadratic for the second, respectively. They are given as follows:

$$\begin{cases} a(x) = 12.87\,x^4 - 37.79\,x^3 + 40.43\,x^2 - 18.35\,x + 3.52 \\ b(x) = -2.92\,x^2 + 4.05\,x - 0.66 \end{cases} \tag{2}$$

The indium dependence of the $In_xGa_{1-x}N$ ternary band gap energy, $E_g(x)$, is given in the literature using the nonlinear quadratic function expressed as follows [30]:

$$E_g^{In_xGa_{1-x}N}(x) = E_g^i(x) = x\,E_g^{InN} + (1-x)\,E_g^{GaN} - 3.8\,x(1-x) \tag{3}$$

Where, E_g^{InN} and E_g^{GaN} are the band gap energies of InN and GaN at room temperature, respectively. The band gap narrowing (BGN) due to high doping level is considered through Klaassen model [31] as follows:

$$\Delta E_g = \alpha\left[Ln\left(\frac{N}{\beta}\right) + \sqrt{\left(Ln\left(\frac{N}{\beta}\right)\right)^2 + \gamma}\right] \tag{4}$$

Where $\alpha, \beta,$ and γ are the constants in Ref. [31].

When a solar cell gets sunlight, only photons with energies more significant than the semiconductor band gap energy are absorbed, creating electron-hole pairs [32]. This parameter determines the cut-off (limit) wavelength of photons useful for carrier formation.

Assuming that the absorbed photon creates a pair electron-hole in the i-layer (Internal Quantum efficiency equals unity), the short circuit current density, J_{sc}, directly proportional to the solar emission spectrum, is defined for the i-layer by the following expression [28]:

$$J_{sc} = \frac{q(1-s)}{hc}\mathscr{X}\int_{\lambda_p}^{\lambda_i(x)}[1 - r(\lambda,x)]..\mathscr{A}(\lambda,x,d)..\mathscr{M}_\lambda^0.\lambda.d\lambda \tag{5}$$

Where:

$$\mathscr{A}(\lambda,x,d) = \sum_{k=1}^{N}\left[1 - e^{[-\alpha_k(\lambda,x).d_k]}\right]e^{-\alpha_k(\lambda,x)\sum_{m<k}d_m} \tag{6}$$

$\mathscr{X}$ is the collection efficiency coefficient, d_k and α_k are the k-layer thickness and corresponding absorption coefficient, $\mathscr{M}_\lambda^0$ is the spectral intensity ($W.m^{-2}.nm^{-1}$), s is the grid-shadowing factor, h is the Planck's constant, c is the light speed in the vacuum, q is the elementary charge, λ is the photon wavelength, $\lambda_p\left(\equiv\frac{1.24}{E_g^p}\right)$ is the p-(top) layerwavelength and $\lambda_i(x)$ is the Indium-mole related i-layer wavelength cut-off given as:

$$\lambda_i(x) = \frac{1.24}{E_g^i(x)}(\mu m) \tag{7}$$

The Indium and wavelength-related reflectance coefficient under normal light incidence is given as follows:

$$r(\lambda,x)=\left[\frac{1-n(\lambda,x)}{1+n(\lambda,x)}\right]^2 \tag{8}$$

The photon energy and In-dependent material refractive index, $n(E, x)$, is given as [28]:

$$n(E,x)=\sqrt{A(x)\frac{2-\sqrt{1+\frac{E}{E_g(x)}}-\sqrt{1-\frac{E}{E_g(x)}}}{\left(\frac{E}{E_g(x)}\right)^2}+B(x)} \tag{9}$$

Where: $E\left(=\frac{hc}{\lambda}\right)$ is the photon energy while $A(x)$ and $B(x)$ are the $In_xGa_{1-x}N$-related coefficient linearly interpolated from those experimentally measured for GaN and InN ($A_{GaN}=9.31, A_{InN}=13.55, B_{GaN}=3.03, B_{InN}=2.05$) [29,33].

The critical figure of merit determining the SC performance is the collection efficiency relative to optical and recombination losses, defined as the ratio of the number of charge carriers contributing to the photovoltaic current to the total number of photogenerated charge carriers. It is given by the following formula [34,35]:

$$\mathscr{X}=\frac{\int_0^L[G(z)-R(z)]dz}{\int_0^L G(z)dz}=1-\frac{\int_0^L R(z)dz}{\int_0^L G(z)dz} \tag{10}$$

Where $R(z)$ and $G(z)$ are, respectively, the recombination and generation rates of charge carriers and L is the thickness of the solar cell device. Generally, the generation rate is firmly absorption profile-dependent. In this work, we restrict ourselves to a high level of illumination, which enables us to assume that the generation rate is constant. ($G(z)=G_0$). The following expression can obtain the recombination rate:

$$R(z)=\frac{n(z)}{\tau_n}+\frac{p(z)}{\tau_p} \tag{11}$$

τ_n and τ_p are the electron and hole capture times by defects, $n(z)$ and $p(z)$ are, respectively, the electron and hole concentrations obtained via the solution of the steady-state continuity and transport equations as reported in Refs. [34,35]. Because the electric field through the i-layer, due to the ionized doping atoms in n- and p-type regions, is constant, the electron and hole concentrations are given by:

$$\begin{cases} n(z)=\dfrac{G_0 l_p \tau_n}{l_p-l_n e^{bL}}\left(1-e^{bz}\right) \\ p(z)=\dfrac{G_0 l_n \tau_p}{l_p-l_n e^{-bL}}\left(e^{bz}-e^{bL}\right) \end{cases} \tag{12}$$

Where: $b=\frac{l_n-l_p}{l_p l_n}=\frac{2}{L_c}$, $l_n=\mu_n\tau_n E_0$ and $l_p=\mu_p\tau_p E_0$ are drift lengths of free electrons and holes. $\mu_{n,p}$ is the charge carrier mobility and E_0 is the built-in electric field, due a p(n)-doping layers, given as following:

$$E_0=\frac{V_{bi}}{d_i}=\frac{k_b T}{qL}Ln\left(\frac{N_a N_d}{n_i^2}\right) \tag{13}$$

Where: N_a, N_d, d_i and n_i are donor and acceptor doping levels in n- and p-type regions and the i-layer thickness and carrier density, respectively. This latter is given as follows [36]:

$$n_i^2=2.31\ 10^{31}\left(m_e^* m_h^*\right)^{3/2}T^3\ exp\left[-\frac{E_g(x)}{k_B T}\right] \tag{14}$$

Where, m_e^* and m_h^* are respectively the InGaNelectron and hole effective masses given as the linear combination of those of InN and GaN, k_B is the Boltzmann constant and T is the absolute temperature. The carrier mobility depends on the impurity concentrations, μ_i, can be obtained based on the Caughey-Thomas's equation [37]:

$$\mu_i=\mu_{min,i}+\frac{\mu_{max,i}+\mu_{min,i}}{1+\left(\frac{N}{N_{g,i}}\right)^{\gamma_i}} \tag{15}$$

In the latter equation, i denotes electron or hole, and $\mu_{min,i}$, $\mu_{max,i}$, $N_{g,i}$ and γ_i Are the material parameters dependent on the specific material alloy while N is the defect density.

In semiconductors, recombination at defects is typically dominant, as described by Shockley-Read-Hall (SRH) lifetimes. The associated lifetime expressed in diffusion length increases for high-quality materials compared to lousy quality. On the contrary, Auger and Band-to-band direct recombination are fundamental processes that become important at high carrier concentrations [38]. Because of Indium aggregation and/or separation, high Indium fractions in InGaN alloys frequently result in low crystalline quality [39]. A high density of drilling dislocations, stacking faults, and V-shaped defects in the III-nitride epilayers deteriorates device performance [39]. As a result, nonradiative recombination is expected to govern the carrier lifetime at room temperature. The non-radiative lifetime through defect-assisted recombination in deep levels, based on SRH theory, can be stated as [38]:

$$\tau_i=\frac{1}{\sigma_i v_{th} N} \tag{16}$$

Where: $v_{th}(=10^7 cm.s^{-1})$ is the thermal velocity at room temperature, $\sigma_n(=2.7\ 10^{-21} cm^2)$ and $\sigma_p(=2.7\ 10^{-14} cm^2)$ are the electron and hole capture cross sections, respectively, and N is the defect density (cm^{-3}) [40].

Additionally, the AM1.5D, AM1.5G and AM0-related open circuit, V_{oc}, can be defined as follows:

$$V_{oc}=\frac{n_I k_B T}{q}Ln\left[1+\frac{J_{sc}}{J_s}\right] \tag{17}$$

Where, n_I is the ideality factor. This latter is typically in the 1.1–1.5 range for real diodes based on III-V materials. In our modeling, we assume n_I to be equal to 1.2 [41].

The reverse bias saturation current density, J_s, measures the leakage of the minority carriers through the p-n junction [41]. This type of leakage is caused by carrier recombination in the neutral regions on either side of the intersection. III-nitride epilayers are significantly more straightforward to grow with their hexagonal c-axis perpendicular to the substrate surface. Still, the buildup of spontaneous and piezoelectric polarization fields along this axis subjects the structure used in optoelectronic devices to built-in solid electric fields that bend their potential profiles and shift electrons and holes in the opposite sense, significantly sinking the device's performance. For PIN thin layer SC with L thickness, the Sah-Noyce-Schokley approximation is valid, and taking into account the spontaneous and piezoelectric polarization effect at the interfaces, the J_s can be expressed as following [42]:

$$J_s=\frac{qL}{\sqrt{\tau_n\tau_p}}n_i.exp\left[\frac{q\rho_p L_p^2}{\varepsilon_i k_B T}\right] \tag{18}$$

The discontinuity of the polarization from either side of the $In_xGa_{1-x}N/In_{0.42}Ga_{0.58}N$ gives rise to polarization charges with interfacial total density depending on the Indium-mole fraction and can be obtained based on the ab initio calculation reported by Fiorentini et al. [43] as:

$$\sigma_s=\left|P^{sp}_{In_xGa_{1-x}N}+P^{pz}_{In_xGa_{1-x}N}-P^{sp}_{In_{.42}Ga_{.58}N}-P^{pz}_{In_{.42}Ga_{.58}N}\right| \tag{19}$$

Because the charges spread near the interfaces, the polarization charges are distributed in a few atomic layers with a thickness of L_p around $1nm$ [44]. Following that, we will assume that the polarization charges can be described by a bulk charge density given as:

$$\rho_p = \frac{\sigma_s}{L_p} \tag{20}$$

The polarization built at the $In_xGa_{1-x}N/In_{0.42}Ga_{0.58}N$ can be calculated using equations listed below from (21) to (24):

$$\begin{cases} P^{sp}_{In_xGa_{1-x}N} = -0.042x - 0.034(1-x) + 0.038x(1-x) \\ P^{pz}_{InN} = -1.373\varepsilon + 7.559\varepsilon^2 \\ P^{pz}_{GaN} = -0.918\varepsilon + 9.541\varepsilon^2 \end{cases} \tag{21}$$

Where ε is the strain expressed according to the lattice parameter of the top and bottom layers and given as:

$$\varepsilon(x) = \frac{a_b - a_t(x)}{a_t(x)} \tag{22}$$

Where the top lattice parameter is given as:

$$a_t(x) = 0.31986 + 0.03862x \tag{23}$$

The piezoelectric polarization dependence versus the In-fraction can be expressed via Vegard's law as follows:

$$P^{pz}_{In_xGa_{1-x}N} = xP^{pz}_{InN}[\varepsilon(x)] + (1-x)P^{pz}_{GaN}[\varepsilon(x)] \tag{24}$$

The Fill Factor, defined as the ratio of the maximum power output to the product of the open circuit voltage and short circuit density current, is another parameter that characterizes the solar cell. According to Green et al. [41], it is defined by the following expression:

$$FF = \frac{\frac{qV_{oc}}{n_i k_B T} - Ln\left(\frac{qV_{oc}}{n_i k_B T} + 0.72\right)}{1 + \frac{qV_{oc}}{n_i k_B T}} \tag{25}$$

The final critical factor is the solar cell's efficiency, which is calculated as the ratio of the generated electricity to input power and is stated as follows [37]:

$$\eta = \frac{V_{oc} \bullet J_{sc} \bullet FF}{P_{in}} \tag{26}$$

Finally, we have chosen to shine on the cell the ASTM G173-03 reference spectra (SMARTS v.2.9.2) from the American Society for Testing and Materials (ASTM) experimental database related to AM1.5D, AM1.5G, and AM0 spectra. Through this paper, different material-dependent parameters for performing our modeling are required. Most of them are summarized in Table 1.

3. Results and discussion

The design n-$In_{0.42}Ga_{0.58}N$/i-$In_xG_{1-x}aN$/n-$In_{0.42}Ga_{0.58}N$structure under investigation is shown in Fig. 1. The three layers constituting the structure under study are as follows: a very thin (Typically *ten nm*) p-type layer, a much thicker (typically a few micrometers) unintentionally doped absorption layer, and a $0.5\mu m$ n-type layer. The p-type $In_{0.42}Ga_{0.58}N$ top layer absorbs all photons for which the energy is more significant than 1.42 *eV* while the intrinsic layer one $In_xGa_{1-x}N$ absorbs those for which the energy is smaller than 1.42 *eV* and more significant than the adjusted intrinsic layer band gap energy ($E_g(x)$: Eq. (3)). Our main goal is to determine the optimum circumstances for unintentionally doped layers, such as In-content, defect concentration, and layer thickness for proper solar cell operation, i.e., to calculate the PV efficiency according to intrinsic parameters. Interestingly, our calculations are carried out under the presumption that the entire area surrounding the structure is flat land with no nearby buildings (Desert). This implies that the shadow parameter is zero (s = 0).

Initially, because the absorption coefficient is vital in calculating different solar cell characteristics, we have shown in Fig. 2 how it varies with wavelength for various In-content values. By increasing the In-content, the intrinsic layer can readily absorb a broad wavelength spectrum from 900 nm to 1900 nm. Additionally, the absorption coefficient is of a magnitude of $10^5 cm^{-1}$ and decreases quickly below the band edge. Furthermore, it can be seen that increasing the In-composition causes the absorbance of low photons, which is advantageous for PIN-based SC. Also, considering the BGN influence due to unintentional and/or intentional doping leads to more broadening of the absorption spectrum toward higher wavelengths. Interestingly, the BGN influence is more prominent than the defect concentration and the in-mole fraction augment.

To have enough components to investigate the behavior of the SC electrical characteristics, particularly the photovoltaic efficiency, in response to various input conditions on the structure, we first deal with the collection efficiency parameter. Its changes versus the intrinsic thickness are illustrated in Fig. 3 for multiple values of defect concentrations (a) and In-mole fractions (b) for n(p)-type doped layer concentration of $10^{18}(10^{17} cm^{-3})$. It is seen that the collection efficiency strongly depends on the intrinsic characteristics (thickness, In-mole, and defect concentrations). This indicates that an effective InGaN alloy must be used for manufacturing high-efficiency sunlight-generating cells. The collection efficiency is practically unity and independent of the intrinsic layer's thickness in the low-defect density range up to $10^{14} cm^{-3}$. Good quality InGaN alloys may exhibit high-collection effectiveness, making them more appropriate for manufacturing powerful solar cells. Generally, a thicker i-layer-related photovoltaic cell leads to a smaller built-in electric field (Eq. (13)) and, as a consequence, shorter drift lengths of free carriers. Even though faster drift lengths make it more difficult for charge carriers to get to the electrodes, good sample quality prevents them from being captured by defects. This enhances the carrier's diffusion to reach the electrodes to be collected. As a result, in a good quality InGaN solar cell, high collection efficiency and a lower defect capture rate were expected. However, it is evident from Fig. 3 that for a high defect density range ($\geq 10^{15} cm^{-3}$), as the i-layer thickness of SC rises, the collection efficiency declines. When the defect density reaches $10^{17} cm^{-3}$, the $In_{.65}Ga_{.35}N$ related collection efficiency falls drastically. Carriers created in the i-layer cannot successfully drift to the device's contacts before recombination, thus failing to contribute to the photocurrent. Consequently, the separated charge carriers were effortlessly captivated by high-density defects, leading to low collection efficiency. Additionally, for fixed defect density and i-layer thickness values, the collection efficiency decreases for high indium-content cells. Generally, high In-content (small band gap) leads to a small built-in electric field (built-in voltage), and the carriers show shorter drift lengths. The In-

Table 1
Material parameters of InN and GaN [45–51].

Parameter	InN	GaN	Parameter	InN	GaN
$E_g(eV)$	0.78	3.42	$\varepsilon^*(\varepsilon/\varepsilon_0)$	10.5	8.9
$m_e^*(m_e/m_0)$	0.07	0.2	$m_h^*(m_h/m_0)$	0.6	1.25
$\mu_{min,e}(cm^2/(V.S))$	30	55			
$\mu_{min,h}(cm^2.Vs^{-1})$	3	3	$\mu_{max,e}(cm^2/(V.S))$	1100	1000
$\mu_{max,h}(cm^2.Vs^{-1})$	340	170	$\gamma_{e(h)}$	1(2)	1(2)
$N_{g,e}(cm^{-3})$	8.10^{17}	2.10^{17}	$N_{g,h}(cm^{-3})$	8.10^{17}	3.10^{17}
$N_C(cm^{-3})$	$9.15.10^{17}$	$1.22.10^{18}$	$N_v(cm^{-3})$	$5.21.10^{19}$	$4.21\ 10^{19}$

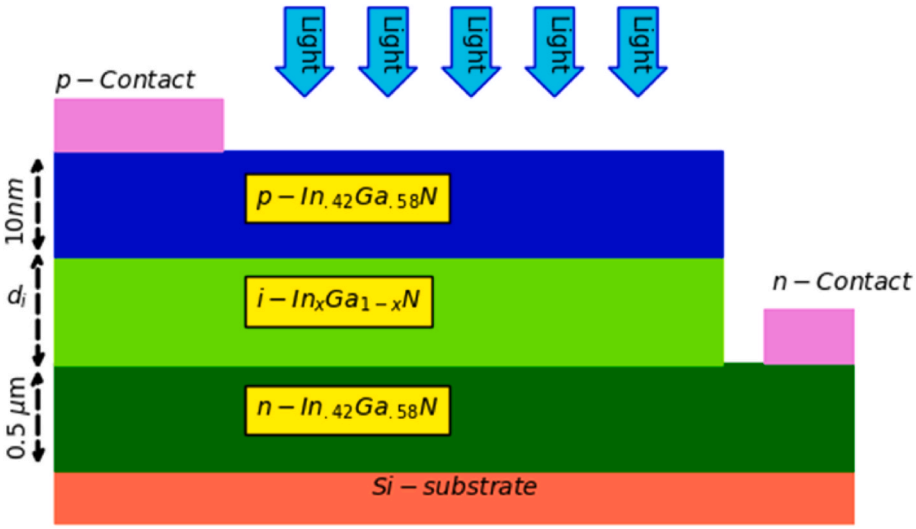

Fig. 1. The solar cell structure under study.

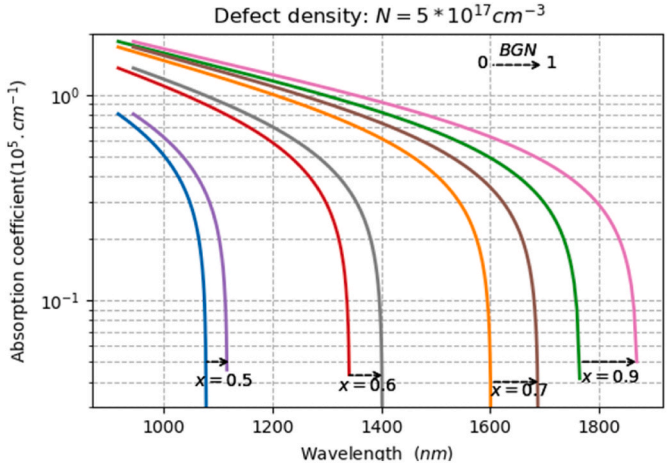

Fig. 2. Semilog plot of the absorption coefficient of the unintentionally doped layer ($In_xGa_{1-x}N$) Versus wavelength for different values of Indium-mole composition ($x \geq 0.43$). The BGN impact is included (0 ≡ Without, 1 ≡ With).

content impact is more marked for thick i-layers than for thin ones.

The variations of the collection efficiency according to i-layer thickness under the effects of n(p)-type doping concentration are illustrated in Fig. 4. Similar behavior is displayed as n(p)-type doped concentration increases. Our modeling results show that increasing the doping concentration increases the collection efficiency, particularly for thick i-layers.

The short circuit current density variations of single homojunction SC are depicted on panels (a) and (b) of Fig. 5 versus the In-composition for three different values of i-layer thickness. As illustrated, J_{sc} shows a strong dependence on the intrinsic characteristics. Our results reveal an integrated maximum short circuit current density for $In_{0.85}Ga_{0.15}N$ intrinsic layer. Also, it can be seen that by increasing the i-layer thickness, J_{sc} Illustrates a nonlinear enhancement. To get a good picture of this behavior, we have reported in Panel (b) the changes of J_{sc} optimum value versus the i-layer thickness for two different values of its defect concentrations. It is clear that whatever the defect concentration, The optimum value of J_{sc} Increases significantly to converge to the saturation regime. Such a behavior can be assigned to the collection efficiency and generation charge carrier's rate for which the product defines J_{sc} as stated in Eq. (5). Additionally, for a fixed i-layer thickness, J_{sc} optimum value increases as the quality of the structure augments (defect density decreases). For instance, it is equal to 17.8 $mA.cm^{-2}$ and 42.1 $mA.cm^{-2}$ for defect concentration of about $10^{16}cm^{-3}$ and $10^{12}cm^{-3}$ respectively, showing an enhancement of about 136.5%. This can be attributed to the inefficient collection, leading to J_{sc} falling when the quality of the structure is degraded. Moreover, it is interesting to mention that as the defect concentration increases, the required thickness decreases to reach the optimum value. For instance, it is equal to $1\mu m$ for defect concentration similar to $10^{12}cm^{-3}$ while it is equal to $0.6\mu m$ for defect concentration equal to $10^{16}cm^{-3}$.

Generally, owing to the logarithmic relationship between V_{oc} and J_{sc}, V_{oc} should exhibit an analogous pattern but with less variation than J_{sc} For cells with identical input conditions. Panel (a) of Fig. 6 illustrates the variations of V_{oc} according to the In-mole fraction of the unintentionally doped layer for three different values of defect concentrations. It is observed that V_{oc} is not monotonic but decreases for vanishing at high in-mole fraction. Our findings show that this critical in-content increases with the enhancement of the structure's quality. For instance, it is equal respectively to 78% and 64% for defect concentration equal to 10^{12} and $10^{14}cm^{-3}$. Compared to J_{sc} results, V_{oc} ones should only be explained by the fact that in PIN SC, the reverse saturation current density enhancement masks that of $J_{sc}(J_{sc}^{''}J_s)$ Which leads to a V_{oc} It is declining, especially for high In-content. This finding correlates with the reality that InGaN PIN homojunction solar cells with higher defect and dislocation densities have a more prominent dark current, leading to lower. V_{oc}. Moreover, the variations of V_{oc} maximum versus the i-layer thickness is illustrated on Panel (b). It is revealed that V_{oc} behavior versus i-layer thickness is strongly governed by that of J_{sc}. Our results don't show significant variations for thicker structures when increasing the i-layer thickness compared to thinner ones. The saturation regime, illustrated in Panel (b), may also be understood as a result of equilibrium between solar light absorption, which rises with thickness, and the carrier's mobility, diffusion length, and collection efficiency, which decline with increasing i-layer thickness. In addition, it is observed that similar behavior is displayed with varying defect concentrations for fixed i-layer thickness. As mentioned earlier, this result can be ascribed to collection efficiency behavior. Our results are more consistent with the J_{sc} trends versus the i-layer thickness and defect concentration.

The obtained results regarding the changes of the fill factor (FF) according to In-mole fraction, thickness, and defect concentration are displayed in Fig. 7. For solar cells with identical input conditions and compared to earlier results of V_{oc}, FF should exhibit similar trends but with fewer changes when adjusting i-layer input parameters. The main feature of Panel (a) is that our modeling results display two different

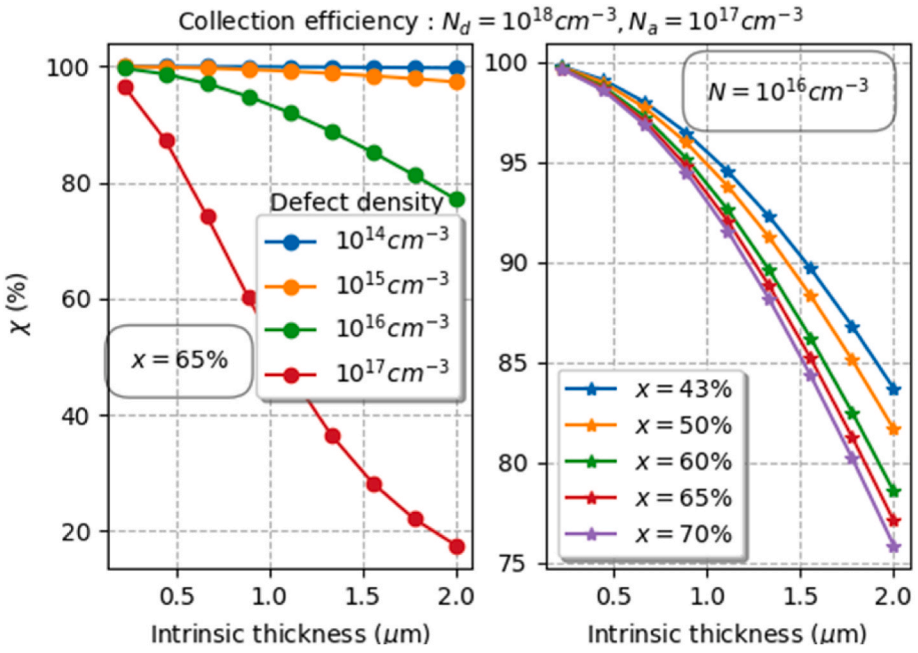

Fig. 3. (Online color) The collection efficiency versus the unintentionally doped layer thickness at room temperature. The impacts of defect concentration (Panel (a)) and Indium-mole composition (Panel (b)) are considered. (For interpretation of the references to color in this figure legend, the reader is referred to the Web version of this article.)

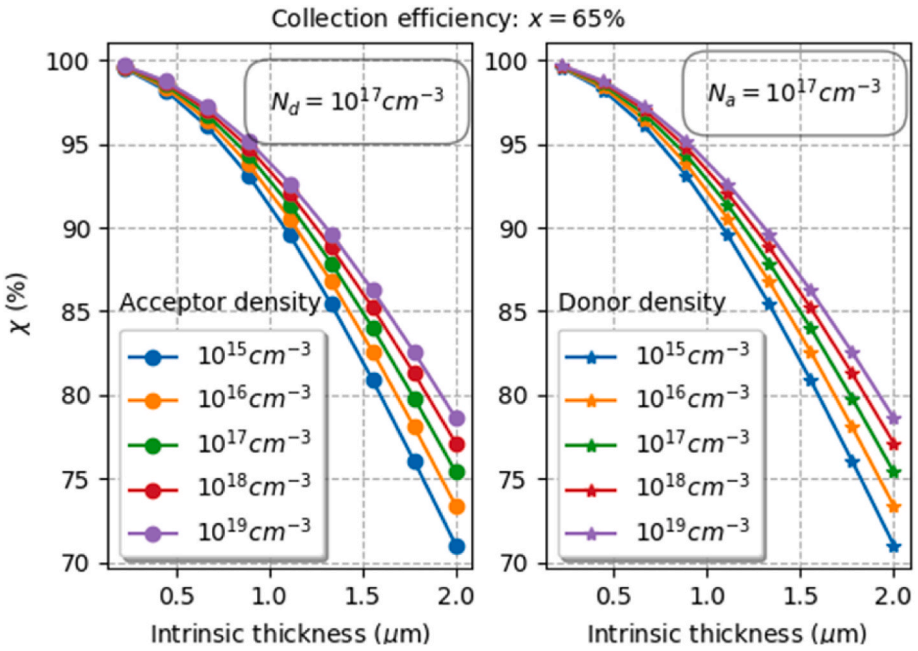

Fig. 4. (Online color) The collection efficiency versus the unintentionally doped layer thickness at room temperature. The impacts of n(p)-type concentration are included. (For interpretation of the references to color in this figure legend, the reader is referred to the Web version of this article.)

behaviors. For low In-content, it appears that with increasing In-fraction, FF decreases to reach a minimum value while remaining intact for high one. It should be noted that the In-critical value depends strongly on defect concentration. For instance, with increasing defect concentration from 10^{12} to $10^{14}cm^{-3}$, the critical minimum value is displaced to lower In-contents from 0.69 to 0.63. It is evident that for high In-content, FF is In-independent and equals 32.8%. Also, Panel (b) revealed that FF is enhanced with increasing the i-layer thickness, particularly for the thinner layer, regardless of the defect concentration. However, it drops as the i-layer quality is degraded apart from its thickness. These results can be understood and interpreted quickly based on those of V_{oc}. Our findings revealed that FF can reach 89% for high-quality structures. $(10^{8}cm^{-3})$ and drops significantly to be equal to 40% for $10^{18}cm^{-3}$ defect concentration (Not shown here). Generally, the FF-related thin films based III-V SC is very high, ranging from $80-86\%$ [52]. Moreover, the reported FF of low-indium InGaN/GaN multiple quantum well (MQWs) solar cells is currently around 72% [53], whereas that of low-indium InGaN PIN homojunction solar cells falls between 64% and 69% [54]. Also, it is reported by Feng et al. [21] that FF can be adjusted within the range of $40-80\%$ as the $2\mu m$-intrinsic layer

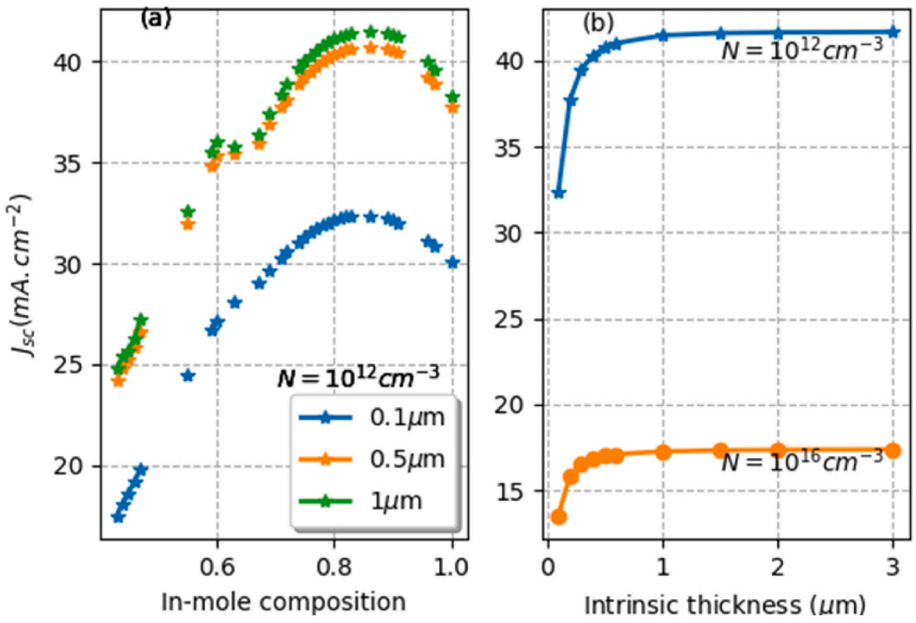

Fig. 5. (Online color) The short circuit current density, J_{sc}, as a function of the In-mole fraction of the unintentionally doped layer at room temperature. The impact of multi-layer thickness is considered. (For interpretation of the references to color in this figure legend, the reader is referred to the Web version of this article.)

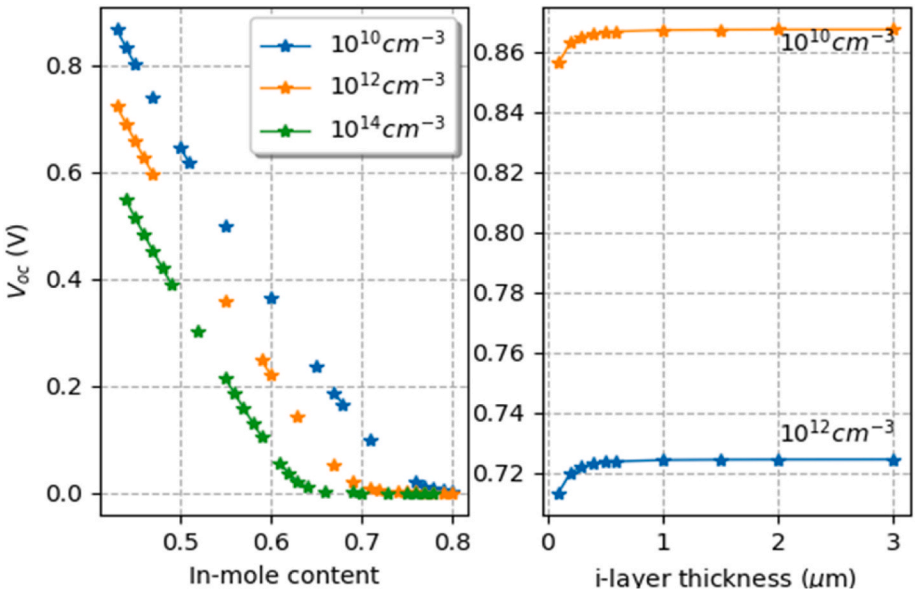

Fig. 6. (Online color) The open circuit voltage, V_{oc}, as a function of the In-mole fraction (Panel (a)) and thickness (Panel (b)) of the unintentionally doped layer at room temperature. The impact of i-layer defect concentration is also considered. (For interpretation of the references to color in this figure legend, the reader is referred to the Web version of this article.)

($In_{0.75}Ga_{0.25}N$) defect concentration varies from 10^{18} to $10^{14} cm^{-3}$.

Fig. 8(a) shows the variations of the PV efficiency versus in-content, whereas Panel (b)shows its changes according to the thickness for different defect concentrations. Compared to V_{oc} and FF results, similar trends are illustrated, demonstrating that these latter are overriding factors when evaluating the effectiveness of PIN InGaN solar cells. Panel (a) shows that whatever the defect density of the i-layer is, the efficiency drops versus the in-content. On the one hand, as In-content increases, the degree of lattice mismatches of the absorber with the p(n)-InGaNtemplates increases, stimulating the possibility of nonradiative recombination due to high defect density formation. This can also be observed via the collection efficiency drop versus In-content. On the other hand, the formation of a heterojunction at the interface of n(p)-InGaN and i-InGaN due to the significant difference in band gap energy, particularly as In-content augments, also disrupts the flow of charge carriers. These enable us to overcome the potential barrier built at the interfaces. These two parameters act in the same sense to reduce efficiency by increasing the intrinsic layer's In-content. Also, it is illustrated that the conversion efficiency vanishes for high In-content regardless of the defect concentration and thickness. This can be only attributed to a considerable value of the reverse saturation current density enhanced by the built-in electric field due to spontaneous and piezoelectric polarizations (Eq. (18)). Moreover, it is interesting to state that the optimal i-layer thickness, as shown in Panel (b), is about of 1μm. This is a result of the trade-off between two effects acting in the opposite sense,i.e., the solar light absorption, rising with the thickness on the one

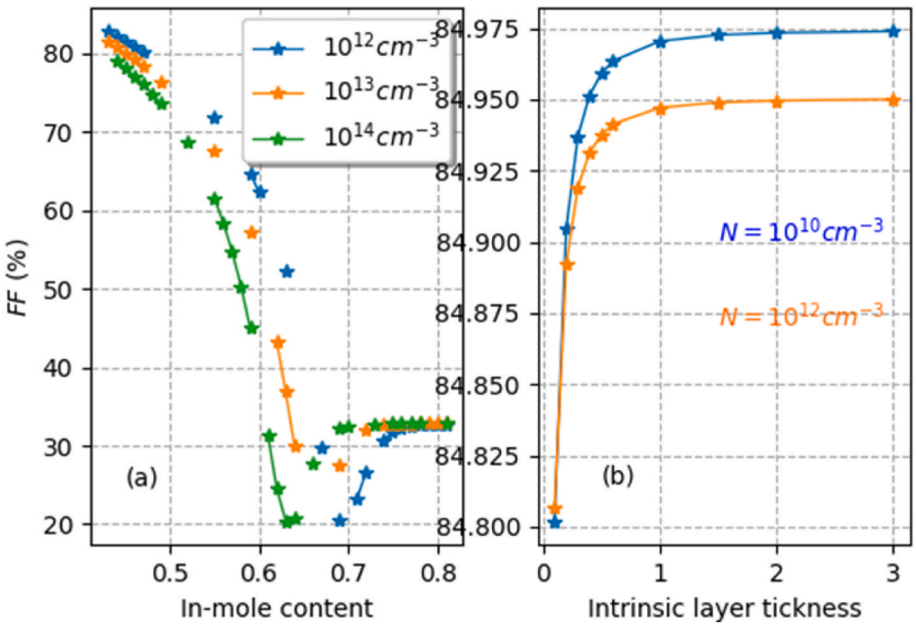

Fig. 7. (Online color) The AM1.5G related fill factor, *FF*, as a function of In-content (Panel (a)) and thickness (Panel (b)) of the unintentionally doped layer at room temperature. The impact of i-layer defect concentration is considered. (For interpretation of the references to color in this figure legend, the reader is referred to the Web version of this article.)

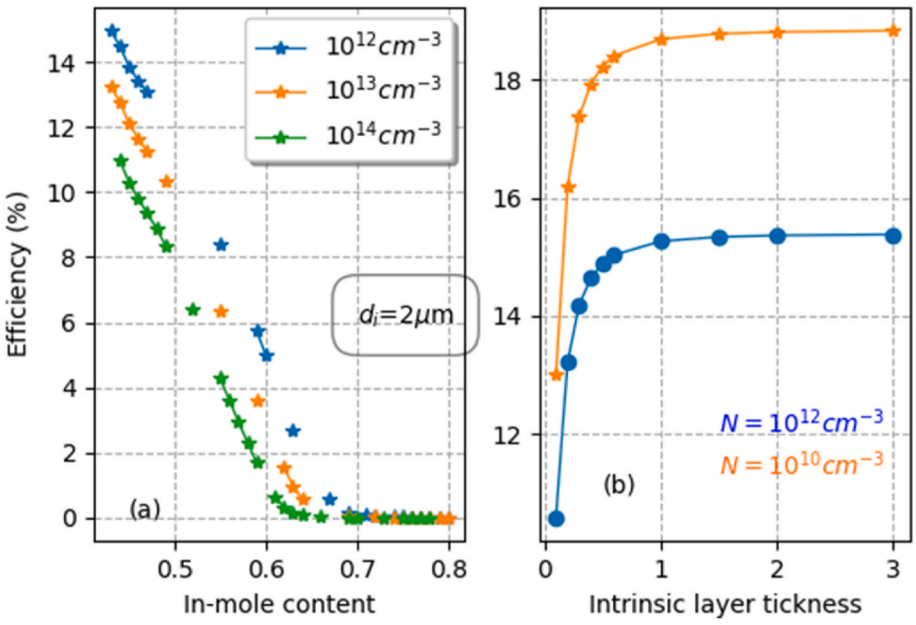

Fig. 8. (Online color) The AM1.5G related photovoltaic conversion efficiency, η, as a function of In-content (Panel (a)) and thickness (Panel (b)) of an unintentionally doped layer at room temperature. The impact of i-layer defect concentration is considered. (For interpretation of the references to color in this figure legend, the reader is referred to the Web version of this article.)

hand, and the carrier's mobility, diffusion length, and collection efficiency that have to remain relatively higher with the increasing-layer thickness on the other hand.

Finally, we present in Fig. 9 the optimum photovoltaic conversion efficiency versus the i-layer thickness of different sun spectra under defect concentration impacts. Notice that the best PV efficiency is obtained for large i-layers regardless of the sun spectrum. Our data show that excellent PV performance is accepted for the AM1.5D spectrum, especially for low defect concentration, while the AM1.5G one is the best as the i-layer quality is degraded. Comparing panels (a) and (b), it is noticeable that the SC performances drastically degrade as the defect concentration increases. For instance, as the defect concentration increases from 10^{12} to 10^{16}cm^{-3}. The AM1.5G-related optimum SC efficiency decreases from 16.5% to 4.12%, showing a declining rate of 75%.

In contrast to some works reported in the literature, our obtained data broadly agrees with the major trends, even if some discrepancies remain due to different material parameters, software-based simulations, and mathematical modeling [12,13,20,21,55,59,60]. For instance, numerical simulation has been performed by Pal et al. [55] to investigate the PIN GaN/$In_xGa_{1-x}N$ heterojunction solar cell. The impacts of In-content in the absorber layer have been studied thoroughly considering polarization charges. The authors reported that the PV

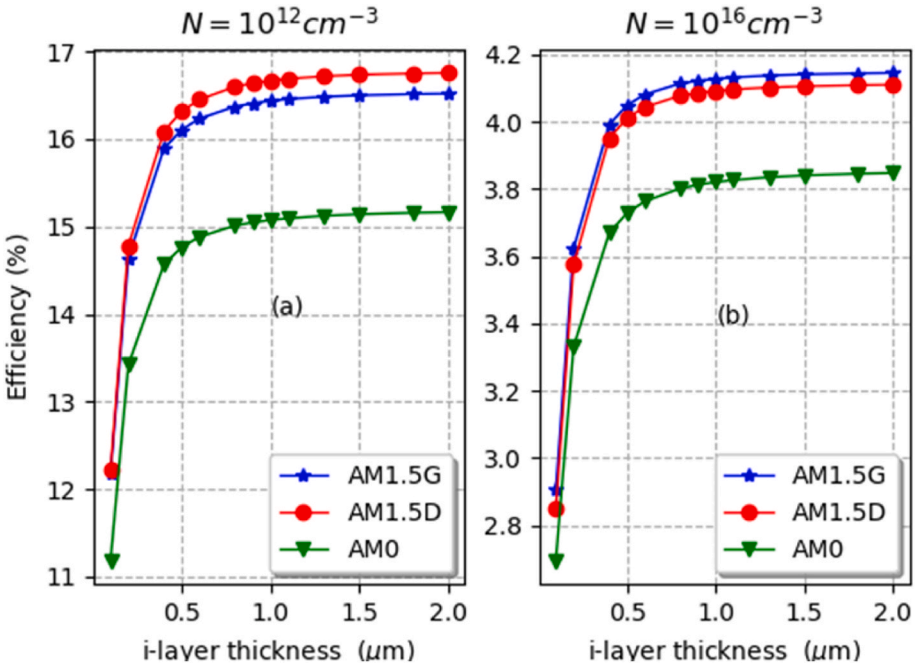

Fig. 9. (Online color) The AM1.5G, AM1.5D, and AM0 related photovoltaic conversion efficiency, η, according to i-layer thickness for two defect concentrations $10^{12}cm^{-3}$ (Panel (a)) and $10^{16}cm^{-3}$ (Panel (b)) at room temperature. (For interpretation of the references to color in this figure legend, the reader is referred to the Web version of this article.)

efficiency increases versus the In-content to reach 4.97% for $0.2\mu m\text{-}In_{0.25}Ga_{0.75}N$ intrinsic absorber. Also, Anirudha et al. [56] calculated p-GaN(5.10^{17})/InGaN/n-GaN(6.10^{18}cm^{-3}) SC characteristics under the impacts of intrinsic parameters. The authors reported that the efficiency increases nonlinearly to reach a value of 4.16% by adjusting the intrinsic layer thickness from 50 up to 550*nm*. Experimentally, Kywahara et al. reported an optimum efficiency of $\eta = 2.5\%$ by growing $In_{0.17}Ga_{0.83}N$ (3 nm)/ $In_{0.07}Ga_{0.93}N$ (0.6 nm) on GaN-substrate with incorporation of $10 \times In_{0.1}Ga_{0.9}N$ (3 nm)/n-GaN (3 nm) to adjust the strains [57]. Similarly, Dahal et al. [58] reported the growth, fabrication, and characterization of SC-based $In_{0.35}Ga_{0.65}N$/GaN MQWs leading to a PV efficiency of about 2.95%. Based on our modeling (Fig. 9), such experimental results, which don't exceed 5%, generally show that defect density (Quality) is the significant disability to obtaining high-efficiency SC. Lastly, when viewed alongside earlier simulation results that did not consider defect density, polarization influences, and collection efficiency, the lower established conversion efficiency confirms that sample quality considerably impacts SC performance and that a high-quality InGaN alloy is necessary for device manufacturing.

4. Conclusion

Numerical modeling was performed to optimize the design and practicability of InGaN p-i-n single homojunction solar cells. A new and efficient model considering the impacts of band gap narrowing, collection efficiency, Shockley-Read-Hall recombination, and interface polarization, which are generally ignored in the literature, is proposed to investigate the PIN solar cells' performance. Summing up our findings, it can be concluded that the defect density, thickness, and indium content of the unintentionally doped layer have essential influences on absorption, collection efficiency, short-circuit current density, open circuit voltage, and conversion efficiency. The combined effects of χ, V_{oc}, J_{ph}, FF and absorption show that the conversion efficiency drops with increasing the In-content up to a critical value. However, the solar cells' efficiency vanishes for high In-content, regardless of the i-layer thickness and quality. Also, our data reveal a $2\mu m\text{-}In_{0.43}Ga_{0.57}N$ AM1.5G-related solar cells optimum efficiency of about $\cong$ 11.3% for $10^{14}cm^{-3}$ defect concentration, which is degraded to $\cong$ 4.15% for $10^{16}cm^{-3}$ one.

CRediT authorship contribution statement

Haddou El Ghazi: Writing – original draft, Investigation, Formal analysis, Conceptualization. **Yasin Ramazan Eker:** Writing – review & editing, Visualization, Validation, Investigation, Formal analysis, Conceptualization. **Redouane En-nadir:** Writing – original draft, Visualization, Validation, Software, Investigation. **Shrouk E. Zaki:** Writing – review & editing, Visualization, Validation, Investigation. **Mohamed A. Basyooni-M. Kabatas:** Writing – review & editing, Writing – original draft, Visualization, Validation, Formal analysis.

Declaration of competing interest

The authors declare that they have no known competing financial interests or personal relationships that could have appeared to influence the work reported in this paper.

Data availability

Data will be made available on request.

Acknowledge

We gratefully acknowledge the support from the National Center for Scientific and Technical Research (CNRST: Morocco) and the Scientific and Technological Research Institution (TÜBİTAK: Turkey) within the joint research project 2543-No: 122N382.

References

[1] Solar Generation 6: Solar Photovoltaic Electricity Empowering the World, 2011, 4 May (2023, http://www.greenpeace.org/international/Global/international/publications/climate/2011/Final%20SolarGeneration%20 VI%20full%20report%20lr.pdf.

[2] Statistica: News release at(https://www.statista.com/statistics/280220/global-cumulative-installed-solar-pv)accessed 4 May (2023).

[3] T.M. Razykov, C.S. Ferekides, D. Morel, E. Stefanakos, H.S. Ullal, H.M. Upadhyaya, Solar photovoltaic electricity: current status and future prospects, Sol. Energy 85 (2011) 1580–1608, https://doi.org/10.1016/j.solener.2010.12.002.

[4] W. Walukiewicz, J.W. Ager, K.M. Yu, Z. Liliental-Weber, J. Wu, S.X. Li, R.E. Jones, J.D. Denlinger, Structure and electronic properties of InN and In-rich group III-nitride alloys, J. Phys. D Appl. Phys. 39 (2006), https://doi.org/10.1088/0022-3727/39/5/R01.

[5] J. Wu, When group-III nitrides go infrared: new properties and perspectives, J. Appl. Phys. 106 (2009), https://doi.org/10.1063/1.3155798.

[6] R.M. Farrell, C.J. Neufeld, S.C. Cruz, J.R. Lang, M. Iza, S. Keller, S. Nakamura, S. P. Denbaars, U.K. Mishra, J.S. Speck, High quantum efficiency InGaN/GaN multiple quantum well solar cells with spectral response extending out to 520 nm, Appl. Phys. Lett. 98 (2011) 2011–2014, https://doi.org/10.1063/1.3591976.

[7] E. Matioli, C. Neufeld, M. Iza, S.C. Cruz, A.A. Al-Heji, X. Chen, R.M. Farrell, S. Keller, S. DenBaars, U. Mishra, et al., High internal and external quantum efficiency InGaN/GaN solar cells, Appl. Phys. Lett. 98 (2) (2011) 021102, https://doi.org/10.1063/1.3540501.

[8] S. Lin, S. Zeng, X. Cai, J. Zhang, S. Wu, L. Sun, B. Zhang, Simulation of doping levels and deep levels in InGaN-based single-junction solar cell, J. Mat. Sci. 47 (11) (2012) 4595–4603, https://doi.org/10.1007/s10853-012-6321-6.

[9] E.N. Afshar, R. Rouhi, N.E. Gorji, Review on the degradation and device physics of quantum dot solar cells, Mod. Phys. Lett. B 29 (1) (2015) 1530008, https://doi.org/10.1142/S0217984915300082.

[10] J. Wu, W. Walukiewicz, K.M. Yu, W. Shan, J.W. Ager, E.E. Haller, H. Lu, W. J. Schaff, W.K. Metzger, S. Kurtz, Superior radiation resistance of In1-xGa xN alloys: full-solar-spectrum photovoltaic material system, J. Appl. Phys. 94 (2003) 6477–6482, https://doi.org/10.1063/1.1618353.

[11] T. Selmi, R. Belghouthi, A novel widespread Matlab/Simulink based modeling of InGaN double heterojunction p-i-n solar cell, Int. J. Energy Environ. Eng. 8 (2017) 273–281, https://doi.org/10.1007/s40095-017-0243-7.

[12] R. Belghouthi, J.P. Salvestrini, M.H. Gazzeh, C. Chevelier, Analytical modeling of polarization effects in InGaN double heterojunction p-i-n solar cells, Superlattice. Microst. 100 (2016) 168–178, https://doi.org/10.1016/j.spmi.2016.09.016.

[13] R. Belghouthi, S. Taamalli, F. Echouchene, H. Mejri, H. Belmabrouk, Modeling of polarization charge in N-face InGaN/GaN MQW solar cells, Mater. Sci. Semicond. Process. 40 (2015) 424–428, https://doi.org/10.1016/j.mssp.2015.07.009.

[14] M. Lourassi, I. Bouchama, N. Bouarissa, Effect of light wavelengths on the non polar InGaN-based thin film solar cells performances using one-dimensional modeling, J. Sci.: Adv. Mater. Devices 4 (2019) 509–514, https://doi.org/10.1016/j.jsamd.2019.08.008.

[15] M. Lourassi, B. Soudini, Simulation of piezoelectric and spontaneous polarization effect on the InGaN/Si tandem solar cell, Optik 127 (5) (2016) 3091–3094, https://doi.org/10.1016/j.ijleo.2015.12.037.

[16] N. Laxmi, S. Routray, K.P. Pradhan, III-Nitride/Si Tandem solar cell for high spectral response: key attributes of auto-tunneling mechanisms, Silicon 12 (10) (2019) 2455–2463, https://doi.org/10.1007/s12633-019-00342-y.

[17] H. EL Ghazi, A. Jorio, Electron-hole transition in spherical QD-QW nanoparticles based on GaN/InGaN/GaN under hydrostatic pressure, Phys. B Condens. Matter 429 (2013) 42–45, https://doi.org/10.1016/j.physb.2013.07.025.

[18] H. El Ghazi, A.J. Peter, Threshold pump intensity effect on the refractive index changes in InGaN SQD: internal constitution and size effects, Phys. B Condens. Matter 462 (2015) 30–33, https://doi.org/10.1016/j.physb.2015.01.014.

[19] H. El Ghazi, A. Jorio, Excited-states of hydrogenic-like impurities in InGaN–GaN spherical QD: electric field effect, Phys. B Condens. Matter 430 (2013) 81–83, https://doi.org/10.1016/j.physb.2013.08.029.

[20] A. Adaine, S.O.S. Hamady, N. Fressengeas, Simulation study of a new InGaN p-layer free Schottky based solar cell, Superlattice. Microst. 96 (2016) 121–133, https://doi.org/10.1016/j.spmi.2016.05.020.

[21] S.W. Feng, C.M. Lai, C.H. Chen, W.C. Sun, L.W. Tu, Theoretical simulations of the effects of the indium content, thickness, and defect density of the i-layer on the performance of p-i-n InGaN single homojunction solar cells, J. Appl. Phys. 108 (2010) 093118, https://doi.org/10.1063/1.3484040.

[22] S. Valdueza-Felip, A. Ajay, L. Redaellia, M.P. Chauva, P. Ruterana, T. Cremel, M. Jiménez-Rodríguez, K. Kheng, E. Monroy, P-i-n InGaN homojunctions (10–40% In) synthesized by plasma-assisted molecular beam epitaxy with extended photoresponse to 600 nm, Sol. Energy Mater. Sol. Cells 160 (2017) 355–360, https://doi.org/10.1016/j.solmat.2016.10.007.

[23] R. Islam, R. Kaysir, J. Islam, A. Hashimoto, A. Yamamoto, MOVPE growth of $In_xGa_{1-x}N$ (x=0.4) and fabrication of homo-junction solar cells, J. Mater. Sci. Technol. 29 (128) (2013), https://doi.org/10.1016/j.jmst.2012.12.005.

[24] X. Cai, Y. Wang, B. Chen, M.-M. Liang, W.-J. Liu, J.-Y. Zhang, X.-Q. Lv, L.-Y. Ying, B.-P. Zhang, Investigation of InGaN p-i-n homojunction and heterojunction solar cells, IEEE Photonics Technol. Lett. 25 (2013) 59, https://doi.org/10.1109/LPT.2012.2227702.

[25] A. Bhuiyan, K. Sugita, A. Hashimoto, A. Yamamoto, lnGaN solar cells: present state of the art and important challenges, IEEE J. Photovoltaics 2 (2012) 276–293, https://doi.org/10.1109/JPHOTOV.2012.2193384.

[26] S.Y. Bae, J.P. Shim, D.S. Lee, S.R. Jeon, G. Namkoong, Improved photovoltaic effects of a vertical-type InGaNIGaN multiple quantum well solar cell, Jpn. J. Appl. Phys. 50 (2011), https://doi.org/10.1143/JJAP.50.092301.

[27] L. Sang, M. Liao, N. Ikeda, Y. Koide, M. Sumiya, Enhanced performance of InGan solar cell by using a SuperThin aln interlayer, Appl. Phys. Lett. 99 (2011) 161109, https://doi.org/10.1063/1.3654155.

[28] A. Luque, S. Hegedus, Handbook of Photovoltaic Science and Engineering, John Wiley & Sons Ltd, 2003, https://doi.org/10.1002/0470014008.

[29] G.F. Brown, J.W. AgerIII, W. Walukiewicz, J. Wu, Finite element simulations of compositionally graded InGaN solar cells, Sol. Energy Mater. Sol. Cells 94 (2010) 478–483, https://doi.org/10.1016/j.solmat.2009.11.010.

[30] R. En-nadir, H. El Ghazi, W. Belaid, A. Jorio, I. Zorkani, Intraconduction band-related optical absorption in coupled (In, Ga) N/GaN double parabolic quantum wells under temperature, coupling and composition effects, Results in Optics 5 (2021) 100154, https://doi.org/10.1016/j.rio.2021.100154.

[31] J.W. Slotboom, H.C. De Graaf, Measurements of bandgap narrowing in silicon bipolar transistors, Solid State Electron. 19 (1976) 857–862.

[32] S.M. Sze, Physics of Semiconductor Devices, John Wiley & Sons, NewYork, 1981, p. 264 (Chap 14).

[33] M. Nawaz, A. Ahmad, A TCAD-based modeling of GaN/InGaN/Si solar cells, Semicond. Sci. Technol. 27 (3) (2012) 035019, https://doi.org/10.1088/0268-1242/27/3/035019.

[34] P. Štulik, H. Singh, A simple method to simulate the influence of defects on the short circuit current in amorphous silicon solar cells, J. Non-Cryst. Solids 226 (1998) 299, https://doi.org/10.1016/S0022-3093(98)00446-3.

[35] J. Hubin, A.V. Shah, Effect of the recombination function on the collection in a p-i-n solar cell, Philos. Mag. B 72 (1995) 589, https://doi.org/10.1080/01418639508240314.

[36] H. Hamzaoui, A.S. Bouazzi, B. Rezig, Sol. Energy Mater. Sol. Cells 87 (2005) 595, https://doi.org/10.1016/j.solmat.2004.08.020.

[37] Y.K. Kuo, J.Y. Chang, Y.H. Chih, IEEE J. Quantum Electron 48 (3) (2011) 367–374.

[38] J. Wu, J. Appl. Phys. 106 (2009) 011101.

[39] Y.S. Lin, K.J. Ma, C. Hsu, S.W. Feng, Y.C. Cheng, C.C. Liao, C.C. Yang, C.C. Chou, C. M. Lee, J.I. Chyi, Appl. Phys. Lett. 77 (2000) 2988.

[40] M.A. Reshchikov, H. Morkoç, J. Appl. Phys. 97 (2005) 061301.

[41] C. Hu, R.M. White, Solar Cells, McGraw-Hill, New York, 1983, p. 21.

[42] Y. Liu, Y. Zhang, Q. Yang, S. Niu, Z.L. Wang, Fundamental theories of piezotronics and piezo-phototronics, Nano EnergyVolume 14 (May 2015) 257–275, https://doi.org/10.1016/j.nanoen.2014.11.051.

[43] V. Fiorentini, F. Bernardini, O. Ambacher, Appl. Phys. Lett. 80 (2002) 1204.

[44] Y. Zhang, Y. Yang, Z.L. Wang, Piezo-Phototronics effect on nano/microwire solar cell, Energy Environ. Sci. 5 (2012) 6850–6856, https://doi.org/10.1039/C2EE00057A.

[45] O. Jani, I. Ferguson, C. Honsberg, S. Kurtz, Design and characterization of GaN/InGaN solar cells, Appl. Phys. Lett. 91 (2007), https://doi.org/10.1063/1.2793180, 132117-1–132117-3.

[46] I. Vurgaftman, J.R. Meyer ., Band parameters for nitrogen containing semiconductor, J. Appl. Phys. 94 (2003) 3675–3696, https://doi.org/10.1063/1.1600519.

[47] W. Walukiewicz, J.W. Ager, K.M. Yu, Z.L. Weber, J. Wu, X.S. Li, R.E. Jones, J. D. Denlinger, Structure and electronic properties of InN and in- rich group III-nitride alloys, J. Phys. D Appl. Phys. 39 (2006) R83, https://doi.org/10.1088/0022-3727/39/5/R01.

[48] Y. Nanishi, Y. Saito, T. Yamaguchi, RF-molecular beam epitaxy growth and properties of InN and related alloys, Jpn. J. Appl. Phys. 42 (2003) 2549–2559, https://doi.org/10.1143/JJAP.42.2549.

[49] R. En-Nadir, H. El Ghazi, A. Jorio, I. Zorkani, Ground-state shallow-donor binding energy in (in,Ga)N/GaN double QWs under temperature, size, and the impurity position effects, J. Modeling and Simulation of Materials 4 (1) (2021) 1–6, https://doi.org/10.21467/jmsm.4.1.1-6.

[50] A.G. Bhuiyan, K. Sugita, A. Hashimoto, A. Yamamoto, InGaN solar cells: present state of the art and important challenges, IEEE J. Photovoltaics 2 (2012) 276–293, https://doi.org/10.1109/JPHOTOV.2012.2193384.

[51] W. Wu, W. Walukiewicz, Band gaps of InN and group III nitride alloys, Superlattice. Microst. 34 (2003) 63–75, https://doi.org/10.1109/JPHOTOV.2012.2193384.

[52] M.A. Green, K. Emery, Y. Hishikawa, W. Warta, Prog. Photovoltaics 17 (2009) 85.

[53] M.J. Jeng, Y.L. Lee, L.B. Chang, J. Phys. D Appl. Phys. 42 (2009) 105101.

[54] X.M. Cai, S.W. Zeng, B.P. Zhang, Fabrication and characterization of InGaN p-i-n homojunction solar cell, Appl. Phys. Lett. 95 (2009) 173504, https://doi.org/10.1063/1.3254215.

[55] D. Pal, S. Das, Numerical simulation of GaN/InGaN p-i-n solar cells: role of interlayers in promoting photovoltaic response, Optik - International Journal for Light and Electron Optics 221 (2020) 165403, https://doi.org/10.1016/j.ijleo.2020.165403.

[56] A.S. Kushwaha, P. Mahala, C. Dhavantri, Optimization of p-GaN/InGaN/n-GaN Double heterojunction p-i-n Solar cell for high efficiency: simulation approach, Int. J. Photoenergy (2014), https://doi.org/10.1155/2014/819637.

[57] Y. Kuwahara, T. Fujii, Y. Fujiyama, T. Sugiyama, M. Iwaya, T. Takeuchi, S. Kamiyama, I. Akasaki, H. Amano, Realization of nitride-based solar cell on freestanding GaN substrate, Appl. Phys. Express 3 (11) (Oct. 2010) 111001, https://doi.org/10.1143/APEX.3.111001.

[58] R. Dahal, J. Li, K. Aryal, J.Y. Lin, H.X. Jiang, InGaN/GaN multiple quantum well concentrator solar cells, Appl. Phys. Lett. 97 (7) (2010) 073115, https://doi.org/10.1063/1.34.

[59] A.A. Faremi, A.T. Akindadelo, M.A. Adekoya, A.J. Adebayo, A.O. Salau, S. S. Oluyamo, P.A. Olubambi, Engineering of window layer cadmium sulphide and zinc sulphide thin films for solar cell applications, Results in Eng. 16 (2022) 100622, https://doi.org/10.1016/j.rineng.2022.100622.

[60] A.M. Ramachandran, M.S. Sangeetha, A.S. Thampi, M. Singh, A. Asok, A comprehensive review on optics and optical materials for planar waveguide-based compact concentrated solar photovoltaics, Results in Eng. 16 (2022) 100665, https://doi.org/10.1016/j.rineng.2022.100665.